

RESEARCH ARTICLE

10.1002/2014WR015493

Key Points:

- The complementary relationship (CR) of evapotranspiration exists in alpine steppe
- Local calibrations reveal the CR pattern in semiarid region of Tibetan Plateau
- CR-based estimation of actual evapotranspiration from semiarid alpine steppe

Correspondence to:

Y. Zhang,
yszhang@itpcas.ac.cn

Citation:

Ma, N., Y. Zhang, J. Szilagyi, Y. Guo, J. Zhai, and H. Gao (2015), Evaluating the complementary relationship of evapotranspiration in the alpine steppe of the Tibetan Plateau, *Water Resour. Res.*, 51, 1069–1083, doi:10.1002/2014WR015493.

Received 24 FEB 2014

Accepted 11 JAN 2015

Accepted article online 19 JAN 2015

Published online 19 FEB 2015

Evaluating the complementary relationship of evapotranspiration in the alpine steppe of the Tibetan Plateau

Ning Ma^{1,2}, Yinsheng Zhang^{1,3}, Jozsef Szilagyi^{4,5}, Yanhong Guo^{1,2}, Jianqing Zhai⁶, and Haifeng Gao¹

¹Key Laboratory of Tibetan Environment Changes and Land Surface Processes, Institute of Tibetan Plateau Research, Chinese Academy of Sciences, Beijing, China, ²University of Chinese Academy of Sciences, Beijing, China, ³CAS Center for Excellence in Tibetan Plateau Earth Sciences, Beijing, China, ⁴Department of Hydraulic and Water Resources Engineering, Budapest University of Technology and Economics, Budapest, Hungary, ⁵School of Natural Resources, University of Nebraska-Lincoln, Lincoln, Nebraska, USA, ⁶National Climate Center, Beijing, China

Abstract The complementary relationship (CR) of evapotranspiration allows the estimation of the actual evapotranspiration rate (ET_a) of the land surface using only routine meteorological data, which is of great importance in the Tibetan Plateau (TP) due to its sparse observation network. With the highest in situ automatic climate observation system in a typical semiarid alpine steppe region of the TP, the wind function of Penman was replaced by one based on the Monin-Obukhov Similarity theory for calculating the potential evapotranspiration rate (ET_p); the Priestley-Taylor coefficient, α , was estimated using observations in wet days; and the slope of the saturation vapor pressure curve was evaluated at an estimate of the wet surface temperature, provided the latter was smaller than the actual air temperature. A symmetric CR was obtained between the observed daily actual and potential evapotranspiration. Local calibration of the parameter value (in this order) is key to obtaining a symmetric CR: α , wet environment air temperature (T_{wea}), and wind function. Also, present symmetric CR contradicts previous research that used default parameter values for claiming an asymmetric CR in arid and semiarid regions of the TP. The effectiveness of estimating the daily ET_a via symmetric CR was greatly improved when local calibrations were implemented. At the same time, an asymmetric CR was found between the observed daily ET_a and pan evaporation rates (E_{pan}), both for D20 aboveground and E601B sunken pans. The daily ET_a could also be estimated by coupling the E_{pan} of D20 aboveground and/or E601B sunken pan through CR. The former provided good descriptors for observed ET_a , while the latter still tended to overestimate it to some extent.

1. Introduction

Quantifying terrestrial evapotranspiration rates (ET_a) is not only critical for understanding how the water cycle interacts between the land and the atmosphere, but is also crucial for sustainable water resource management, and thus ecological and environmental conservation in semiarid and arid regions where the water crisis is most severe [Wang and Dickinson, 2012]. The Tibetan Plateau (TP), the world's highest plateau, with an average altitude exceeding 4000 m above sea level (asl), is vitally important to the Northern Hemisphere's climate due to its thermodynamic influence on atmospheric circulation patterns [Wu et al., 2012; Ye and Wu, 1998]. ET_a in the TP therefore plays a key role in hemispheric energy and water cycle at various temporal and spatial scales through the release of latent heat. Consequently, research on ET_a using in situ observations [Biermann et al., 2014; Gu et al., 2008], remote sensing techniques [Chen et al., 2013; Ma et al., 2014], and land surface models [Yang et al., 2011; Yin et al., 2013] at different spatial and temporal scales has intensified in the TP over the past few years. Owing to a harsh environment, only a sparse observation network exists, hindering a reliable estimation of the spatial variation of ET_a within the TP. Specifically, existing meteorological stations managed by the Chinese Meteorological Administration (CMA) [see Yin et al., 2013, Figure 1], and the in situ observatories for land-atmosphere interactions [see Ma et al., 2008, Figure 1], still form an extremely sparse and unevenly distributed network: most stations are located in the eastern and southern TP, with only a few in the western regions. In addition, most stations are in valleys at a relatively low elevation and currently no station is located higher than 4800 m asl [Qin et al., 2009]. Undoubtedly, deriving regionally representative ET_a rates with such scarce data is an obvious challenge, albeit urgent. For instance, the predominant cover of alpine steppe in the central and western TP has experienced significant degradation in the past decade due to changes in precipitation and the melting of frozen soil

[Gao *et al.*, 2010; Zou *et al.*, 2002]. However, little knowledge of the relevant hydrological processes, especially the ET_a of the alpine steppe, has emerged until recently.

Generally, ET_a can be directly measured by lysimeters, scintillometers, the energy balance Bowen ratio, and/or eddy covariance techniques [Allen *et al.*, 2011; Wang and Dickinson, 2012], but these methods require expensive instrumentation and expert labor. The latter requirement is the most challenging in the TP because of its extremely inclement environment. Although recent developments in remote sensing have greatly boosted our knowledge of regional-scale ET_a rates [Chen *et al.*, 2013; Ma *et al.*, 2014], most remote-sensing-based methods only provide us with instantaneous ET_a values. Upscaling of these instantaneous values for longer time periods remains a task [Lhomme and Elguero, 1999]. For the purpose of obtaining ET_a rates over longer periods, the complementary relationship (CR) of Bouchet [1963], based on a proposed complementary feedback mechanism between ET_a and its potential maximum rate, ET_p , under the same environmental conditions, is of value. The CR makes it possible to estimate ET_a from routinely measured meteorological variables, without requiring any major instrumentation. It also dispenses with measuring vegetation and soil conditions, arduous tasks in remote areas. Application of the CR at the catchment/basin scale is very convenient since it bypasses the collection of multiyear precipitation and runoff data to calculate ET_a with the help of a water balance approach. As a result, the CR theory has been applied to quantify ET_a on a wide range of spatial scales from a few kilometers [Huntington *et al.*, 2011; Liu *et al.*, 2012; Kahler and Brutsaert, 2006; Mallick *et al.*, 2013] to basin-size [Liu *et al.*, 2006; Matin and Bourque, 2013; Wang *et al.*, 2011], as well as temporal scales from annual [Hobbins *et al.*, 2004; Ramirez *et al.*, 2005], to monthly [Szilagyi and Jozsa, 2008, 2009a; Szilagyi *et al.*, 2009; Hobbins *et al.*, 2001b; Xu and Singh, 2005], daily [Han *et al.*, 2013; Jaksa *et al.*, 2013; Ozdogan and Salvucci, 2004], or subdaily [Crago and Crowley, 2005; Han *et al.*, 2014; Parlange and Katul, 1992].

Nevertheless, whether the CR could be applied to estimate ET_a in the TP is a matter of debate. On the one hand, it is well established that ET_a and ET_p exhibit an inverse relationship in water-limited areas [e.g., Golubev *et al.*, 2001; Hobbins *et al.*, 2001a, 2004; Jaksa *et al.*, 2013; Ramirez *et al.*, 2005]. Previous research in arid, semiarid, and other regions have demonstrated that the CR-estimated ET_a rates are realistic when compared with water-balance-based [e.g., Hobbins *et al.*, 2001b; Liu *et al.*, 2006; Ozdogan and Salvucci, 2004; Wang *et al.*, 2011] and eddy-covariance-based [e.g., Han *et al.*, 2013, 2014; Liu *et al.*, 2012; Mallick *et al.*, 2013, 2014] approaches. Recently, Brutsaert [2013] also confirmed the existence of an inverse trend between pan evaporation and ET_a in the TP using the CR. On the other hand, several researchers have argued that the CR deviated from Bouchet's [1963] theory to a considerable extent in the arid and semiarid regions of the TP [Wang *et al.*, 2013; Yang *et al.*, 2011; Zhang *et al.*, 2007]. Yu *et al.* [2009] ascribed this deviation to the limited vapor transfer potential at high altitudes because low air temperatures lead to low vapor pressure deficits. However, these studies did not apply locally calibrated parameter values. Applying the original parameter values most frequently encountered in the CR studies for the TP, where solar radiation and the wind are stronger but temperatures are lower, can lead to substantial errors, as was pointed out by Brutsaert [2013]. In fact, calibration of the CR parameter values at a regional basis may be important not only in the TP, but also in other regions. For instance, Xu and Singh [2005] and Hobbins *et al.* [2001b] concluded that the original parameter values of the CR would lead to evidently biased ET_a estimates in comparison with water-balance-derived ET_a values in the semiarid region of Cyprus and in the 139, only minimally altered, basins of the U.S., respectively.

With regard to vegetation cover, the CR approach has been tested in shrublands [Huntington *et al.*, 2011; Jaksa *et al.*, 2013], prairie [Crago and Crowley, 2005; Kahler and Brutsaert, 2006; Szilagyi, 2007], and cropland [Liu *et al.*, 2012; Mallick *et al.*, 2013; Ozdogan and Salvucci, 2004] over the past decade. These works have advanced our understanding of the CR theory involving different vegetation types, but not in conditions that exist in high altitudes. Consequently, with the help of the highest in situ automatic climate observation system in the alpine steppe region of the TP, the objectives of the present study are as follows. (1) Testing the existence of the CR in a high-altitude semiarid alpine steppe ecosystem. (2) Determination of the local parameter values of the CR to estimate daily evapotranspiration rates for the semiarid region of the TP. (3) Exploration of the specific relationship between observed daily ET_a and its maximum potential rate, the latter estimated with the help of evaporation pans as well as with the Penman equation [Penman, 1948]. (4) Evaluation of the CR-estimated daily actual evapotranspiration values.

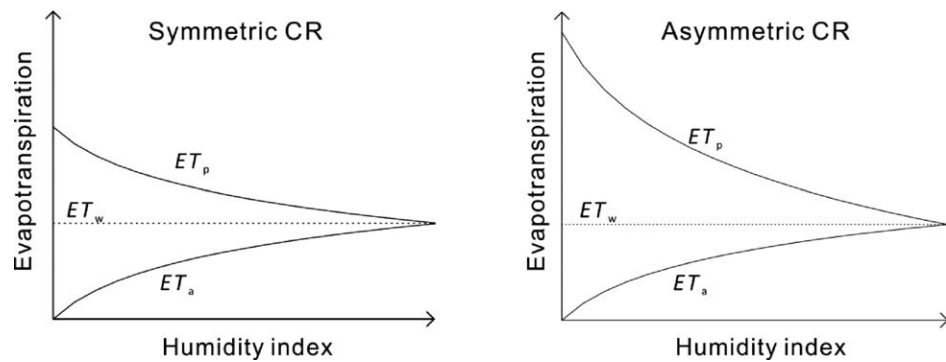


Figure 1. Conceptual representation of the symmetric and asymmetric complementary relationship. ET_a , ET_p , and ET_w are actual, potential, and wet environment evapotranspiration, respectively.

2. Background of the Complementary Relationship

The complementary relationship of evapotranspiration was initially advanced by *Bouchet* [1963], emphasizing the feedback mechanism between ET_a and ET_p over a homogeneous area with minimum advection. Given a homogeneous surface with ample moisture, $ET_a = ET_p = ET_w$, where ET_w is the wet environment evapotranspiration. Differentiation between ET_p and ET_w stems from the horizontal extent of the relevant wet area over which they are defined. For ET_w , it is large enough to modify its environment significantly. With limited water availability, ET_a decreases. The energy that would have been consumed by ET_a thus becomes sensible heat, thereby increasing ET_p , i.e.,

$$ET_p - ET_w = \varepsilon (ET_w - ET_a) \tag{1}$$

where ε is a coefficient that depicts the proportion of the sensible heat that increases ET_p . When ε equals unity, the unit decrease of ET_a yields a corresponding unit increase of ET_p , signifying a symmetric CR (Figure 1a). This is the case for the widely applied advection-aridity (AA) model proposed by *Brutsaert and Stricker* [1979]. However, if the actual wet surface is too small (or too large) and/or some additional heat transfer exists (e.g., through the side and bottom of an evaporation pan), thereby altering the energy flux rate available for the wet surface, the rate of decrease in ET_a would differ from the rate of increase in ET_p . In this case, ε would deviate from unity, creating an asymmetric CR (Figure 1b). It should be noted that a strictly symmetric CR may be difficult to achieve due to the numerous limits imposed by actual conditions. *Sugita et al.* [2001] demonstrated that ε can be expected to equal unity only when soil moisture is ample enough and the evaporation surface is largely smooth. *Pettijohn and Salvucci* [2006] suggested that surface conductance would affect the symmetry of the CR especially when transpiration accounts for a large part of ET_a . In addition, when evaporation of class-A pan was employed as a proxy for ET_p (the pan coefficient was assumed to be unity), *Kahler and Brutsaert* [2006] demonstrated that ε ranged between 4.33 and 6.88 and subsequent numerical experiments by *Pettijohn and Salvucci* [2009] also obtained similar values. *Szilagy and Jozsa* [2009b] stressed the importance of the size of the wet surface the mean evapotranspiration rate is defined for as ET_p , as local ET_p rates change with distance across the dry-to-wet transition.

3. Normalized CR and Practical Applications of ET_p and ET_w

Following *Brutsaert* [2005], one can normalize the ET_a and ET_p values by dividing (1) with ET_w to obtain dimensionless expressions, i.e.,

$$\frac{ET_a}{ET_w} = \frac{(1 + \varepsilon) \frac{ET_a}{ET_p}}{1 + \varepsilon \frac{ET_a}{ET_p}} \tag{2}$$

$$\frac{ET_p}{ET_w} = \frac{1 + \varepsilon}{1 + \varepsilon \frac{ET_a}{ET_p}} \tag{3}$$

Under water-limited conditions, the (ET_a/ET_p) term of (2) and (3) is mainly dependent upon the soil moisture and vegetation cover and could therefore be regarded as a land surface humidity index,

namely $ET_{HI} = ET_a/ET_p$ [Brutsaert, 2005; Kahler and Brutsaert, 2006]. On a daily scale, Kahler and Brutsaert [2006] found that ET_{HI} is better than the total soil moisture content or antecedent precipitation index in capturing the availability of land surface moisture. By using the notation $ET_a/ET_w = ET_{a+}$, $ET_p/ET_w = ET_{p+}$, and $ET_a/ET_p = ET_{HI}$, (2) and (3) can be written as

$$ET_{a+} = \frac{(1 + \varepsilon)ET_{HI}}{1 + \varepsilon ET_{HI}} \quad (4)$$

$$ET_{p+} = \frac{1 + \varepsilon}{1 + \varepsilon ET_{HI}} \quad (5)$$

According to Brutsaert and Stricker [1979], the ET_p term can generally be defined by the Penman [1948] equation

$$ET_p = \frac{\Delta(R_n - G)}{(\Delta + \gamma)} + \frac{\gamma f(U)(e_o - e_a)}{(\Delta + \gamma)} \quad (6)$$

where Δ is the slope of the saturation vapor pressure curve at air temperature ($\text{kPa } ^\circ\text{C}^{-1}$), γ is the psychrometric constant ($\text{kPa } ^\circ\text{C}^{-1}$). R_n and G are net radiation and soil heat flux into the ground in units of mm d^{-1} . e_o and e_a are the saturation and actual vapor pressure of the air (kPa), respectively. $f(U)$ is the so-called Rome wind function [Brutsaert, 1982]

$$f(U) = 2.6(1 + 0.54U_2) \quad (7)$$

a modification of Penman's [1948] original empirical linear equation. U_2 is the wind speed (m s^{-1}) at 2 m height and $f(U)$ is given in $\text{mm d}^{-1} \text{ kPa}^{-1}$.

Similarly, pan evaporation (E_{pan}) can also be regarded as an indicator of ET_p , i.e.,

$$ET_p = cE_{\text{pan}} \quad (8)$$

where c is the so-called pan coefficient. The value of c depends not only on the environmental conditions but also on the pan type. There are a series of values for c for different pans around the world in the literature [e.g., Brutsaert, 2013; Pettijohn and Salvucci, 2009]. However, Kahler and Brutsaert [2006] are followed in adopting a value of unity for it ($c = 1$) in the present study. The same was also employed by Szilagyi [2007] and Pettijohn and Salvucci [2009]. The reasons for this assumption are twofold: (i) one of the goals of the present study is the evaluation of pan evaporation as ET_p within the CR theory, rather than the calibration of c for a specific pan type or area within the TP; (ii) when ET_p is replaced by cE_{pan} in equation (1), the uncertainty of the CR-based method of estimating ET_a could be compensated by the calibration of ε , as was pointed out by Kahler and Brutsaert [2006].

ET_w is closely approximated by the Priestley-Taylor equation [Priestley and Taylor, 1972] because it is mostly a function of available energy ($R_n - G$), satisfying the concept of wet environment evapotranspiration as defined by Bouchet [1963]

$$ET_w = \alpha \frac{\Delta(R_n - G)}{\Delta + \gamma} \quad (9)$$

Here ET_w is the wet environment evapotranspiration rate (mm d^{-1}), α is the dimensionless Priestley-Taylor coefficient, commonly having a default value of 1.26 [Priestley and Taylor, 1972], while other variables remain as in (6).

4. Site Description, Measurement, and Data Preparation

Alpine steppe is a very typical land cover in TP. It occupies nearly 1/3 of TP with total area of $\sim 800,000 \text{ km}^2$ [Miehe et al., 2011]. From a climatological point, it is principally distributed in the frigid and dry areas of TP [Yang et al., 2009] with altitude ranging from 4500 to 5500 m asl [Wang et al., 2014]. In the present research, an automatic climate observation system (ACOS) was established in September 2011 in the Shanghu alpine steppe (SAS) area (Figure 2), the hinterland of the Qiangtang plateau of the TP. The altitude of the observation site is 4947 m asl. Present alpine steppe was dominated by *Stipa purpurea* and *Carex moocroftii*. In the growing season, the mean canopy height and vegetation coverage are 0.03 m and 30%, respectively. The

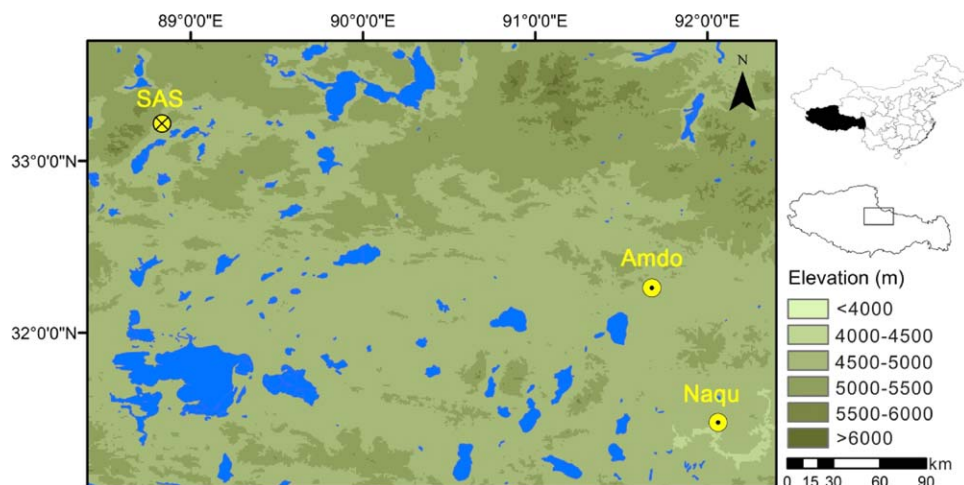


Figure 2. Location of the in situ observations (SAS) in a typical semiarid alpine steppe area and the two other China Meteorological Administration stations at Naqu and Amdo, where pan evaporation observations were made. The blue areas denote lakes of the TP.

soil of the homogeneous, flat area around ACOS, with a fetch in excess of 1 km for the prevailing wind is predominantly sandy loam. This region is characterized by a frigid semiarid climate [Zheng *et al.*, 2013]. ACOS records reveal a mean annual temperature of $\sim -4^{\circ}\text{C}$ from October 2011 to September 2013, with July temperatures of about 7°C , down to approximately -15°C in January. Records from the CMA station closest to the SAS reported annual precipitation of ~ 333 mm [Zheng *et al.*, 2013] and annual ET_p of ~ 1000 mm [Wang *et al.*, 2013]. The rainy season (June to September) accounts for more than 85% of the total annual precipitation. Since the glacier equilibrium line altitude in this region is roughly 5800 m asl [Yao *et al.*, 2012], the present research represents the highest altitude in situ observations made in the alpine steppe ecosystem.

Table 1 displays details of the in situ observations of air temperature/humidity, pressure, wind speed/direction, radiation, soil heat flux, and soil temperature. All data were obtained as 10 min averages. Since the soil heat flux plate measured soil heat flux at a depth of 0.03 m, the temperature integration method [Oliphant *et al.*, 2004] was used to interpolate heat storage between 0 and 0.03 m, using soil temperatures at depths of 0 and 0.05 m. Thus, the ground heat flux values, G , in the present study indeed represent heat fluxes into the ground surface rather than at a depth of 0.03 m. G accounted for $\sim 7\%$ of R_n at SAS on average (June to September), which is consistent with the theoretical proportion [Brutsaert, 2005], indicating reliable observational data.

In order to eliminate high-frequency noise, the raw 10 min measurements were processed to half-hourly average values. Then the half-hourly ET_a values were derived using the energy balance Bowen ratio method [Allen *et al.*, 2011]. Finally, the 48 half-hourly ET_a values of the day were aggregated to calculate daily ET_a . Although the recommended period of the CR application is 3–5 days [Morton, 1983], recent research indicate that daily ET_a can also be estimated accurately by CR theory [Han *et al.*, 2013, 2014; Kahler and Brutsaert, 2006], consequently all evaluations in the present study are performed on a daily basis. Our aim is to investigate ET_a in the growing season (from October to May air temperature is typically below 0°C , and precipitation as well as plant physiological activity are also at a minimum). Data in the present study are therefore taken from the period of 4 June to 30 September in 2012 and 2013.

Table 1. Specifics of the In Situ Observations in the SAS

Observed Items	Height/Depth (m)	Sensor Type/ Manufacturer/Country
Air temperature/ humidity	0.7, 1.5, 2, 4	HMP45C, Vaisala, Finland
Air pressure	0.5	PTB100, Vaisala, Finland
Wind speed	0.7, 1.5, 2, 4	010C-1, MetOne, USA
Wind direction	4	020C-1, MetOne, USA
Net radiation	0.7	CNR4, Kipp & Zonen, Netherlands
Soil heat flux	0.03	HFP01SC, Hukseflux, Netherlands
Soil temperature	0, 0.05	109, Campbell Scientific, USA

Note that the observations (including pan evaporation data below) of 2013 were used to calibrate the parameter values in sections 5 and 6, while data of 2012 were employed to test the effectiveness of the CR-based method in estimating the daily actual evapotranspiration rates in section 7.

As was mentioned above, pan evaporation is a proxy of ET_p . Daily pan

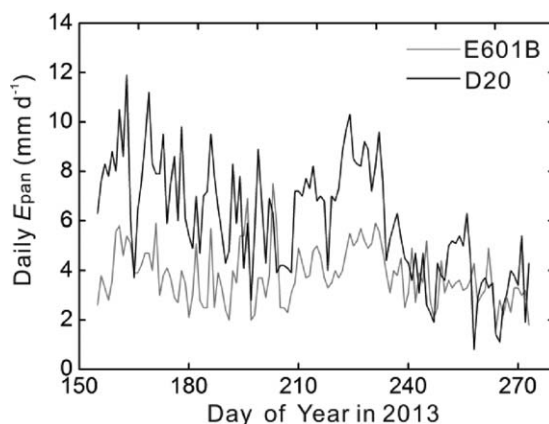


Figure 3. Comparison of the daily E601B sunken pan evaporation (Naqu) and D20 above ground pan evaporation (Amdo) from 4 June 2013 to 30 September 2013 (155th–273rd day of year).

Amdo is the China D20 model (for a photo, see Figure 2 in Yang and Yang [2012]), made of copper with a depth of 0.1 m and a diameter of 0.2 m. The D20 pan is installed on a platform 0.7 m above the ground and has a rim acting as a bird guard. According to the WMO's [2008] pan classification, the E601B pan (at Naqu) is a sunken pan, while the D20 pan (at Amdo) is an aboveground pan. Although these two stations are located at a somewhat lower altitude than SAS, the climatological background of both Naqu and Amdo are comparable to that of the SAS [Zheng et al., 2013]. It is therefore assumed that the main environmental factors influencing the pan evaporation rates at these stations and the actual ET_a rates at the SAS are, to a large extent, similar. Figure 3 displays the variation of daily E_{pan} of these two stations from 4 June to September in 2013. The variability of the E_{pan} rates at these two stations match well, however, their magnitude express an obvious difference.

evaporation data from the same period (4 June to 30 September in 2012 and 2013) of two CMA meteorological stations in the relative vicinity of SAS were also utilized. One is the station at Naqu (28.71°N, 92.06°E, 4520 m asl, Figure 2), the other is at Amdo (32.25°N, 91.67°E, 4690 m asl, Figure 2), located 360 and 290 km to the southeast of the SAS, respectively. The pan at the Naqu is the China E601B model (for a photo, see Figure 1 in Ohmura and Wild [2002]), which is similar to the Russian GGI-3000 pan [World Meteorological Organization (WMO), 2008]. It is made of fiberglass with a depth of 0.687 m and a diameter of 0.618 m. The E601B pan is buried in the soil with its orifice 0.3 m above the ground surface [Xiong et al., 2012]. The pan at

5. Local Calibration and Verification of the Key Parameter Values in CR at SAS

5.1. Alternative Formulation of the Wind Function for Calculating ET_p

Although the original wind function of Penman [1948] does not require boundary layer flow characterization, the ability of (6) with (7) to describe ET_p accurately may depend on local environmental conditions. Linacre [1993] suggested that any wind function should be expressed by a certain range rather than a fixed formula. As both ET_p and E_{pan} rates are sensitive to wind speed in water-limited environments [Hobbins et al., 2001b; van Heerwaarden et al., 2010], it may be necessary to replace (7) with a more appropriate method. For daily (or longer) periods, atmospheric stability is often assumed to be neutral, hence Brutsaert and Stricker [1979] suggested the calculation of $f(U)$ via the Monin-Obukhov Similarity (MOS) theory [Monin and Obukhov, 1954] as

$$f(U) = \frac{0.622k\rho U_*}{P \ln \left[\frac{z_1 - d}{z_{0v}} - \psi_v \right]} t \tag{10}$$

$$U_* = \frac{U_{z_2} k}{\ln \left[\frac{z_2 - d}{z_{0m}} - \psi_m \right]} \tag{11}$$

where k is the von Karman constant (0.4), ρ is the density of air (kg m^{-3}), P is the air pressure (kPa), $t = 1 \text{ d} = 86,400 \text{ s}$, and z_1 is the height of humidity measurements (2 m in the present study). d is displacement height (m), often taken to be $2h/3$ [Brutsaert, 2005], where h is the mean canopy height (0.03 m at SAS). U_* is the friction velocity (m s^{-1}), U_{z_2} is the wind speed (m s^{-1}) at a height of z_2 (2 m in the present study), and z_{0m} is momentum roughness length (m) assumed to equal $h/8$ [Brutsaert, 2005]. z_{0v} is the water vapor roughness length (m) and typically expressed as $z_{0v} = z_{0m} \exp(-kB^{-1})$, where kB^{-1} is a dimensionless number and can be assumed to equal 2 for a homogeneously vegetated surface [Pettijohn and Salvucci,

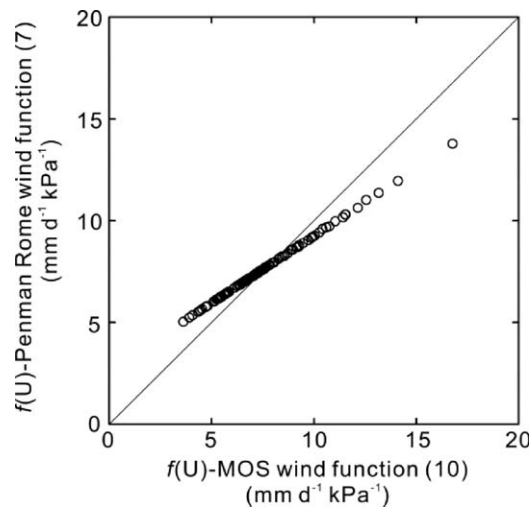


Figure 4. Comparison of the MOS-based (10) and Penman Rome (7) wind functions at 2 m above the ground at SAS.

estimates it in stronger winds. Based on our observations, 67% of the daily wind speed values from June to September in 2013 at SAS were less than 3.7 m s^{-1} . This suggests that the Penman Rome wind function (7) probably overestimates $f(U)$ (and hence ET_p) in most days of the growing season at SAS. In order to distinguish ET_p based on (6) and (7), we denoted potential evapotranspiration as “ ET_{p-c} ” when the estimate was based on (6), with $f(U)$ calculated by the MOS method (10).

5.2. Local Derivation of Δ and α for Calculating ET_w

Since the Priestley-Taylor equation’s parameter value, α , was calibrated in a wet environment [Priestley and Taylor, 1972], Szilagyi and Jozsa [2008] proposed that the Δ in (9) should be evaluated at the air temperature of the wet environment (T_{wea}) rather than the actual air temperature (T_a). This modification is especially significant when it is applied in arid/semiarid regions because of the possible large difference between T_{wea} and T_a under water-limited conditions [Huntington et al., 2011]. Also, previous studies have indicated that Brutsaert and Stricker’s [1979] AA model, based on a symmetric CR, tends to overestimate ET_a in arid and semiarid regions when ET_w is evaluated by T_a [Szilagyi et al., 2009; Szilagyi and Jozsa, 2008] since an overestimation of ET_w also yields an overestimation of ET_a as can be seen from (1)—applying $\varepsilon = 1$ —after rearrangement [Huntington et al., 2011], viz. $ET_a = 2ET_w - ET_p$.

Unfortunately, it is not straightforward to determine T_{wea} from nonhumid observations. Szilagyi and Jozsa [2008] proposed obtaining T_{wea} by approximating it with the wet environment surface temperature, T_{wes} , of a plot-sized wet patch, surrounded by water-limited conditions (arguing that the T_{wes} of the small wet patch is the same as that of an extensive wet area over which an equilibrium vertical temperature profile with typically small gradients develops, hence $T_{wes} \approx T_{wea}$) as

$$\beta_{we} = \frac{Rn - G - ET_{p-c}}{ET_{p-c}} \approx \gamma \frac{T_{wes} - T_a}{e_o(T_{wes}) - e_a} \quad (12)$$

where β_{we} is the Bowen ratio of the wet patch (assuming that available energy for the wet patch is close to that of the drying surface), T_a is the actual air temperature in the surrounding water-limited environment, with actual vapor pressure of e_a at T_a , and $e_o(T_{wes})$ being the saturated vapor pressure at T_{wes} ($\approx T_{wea}$), respectively. Equation (12) works, because over a small wet patch, air temperature and vapor pressure are only minimally affected by the presence of the wet surface, allowing for insertion of the measured, water-limited T_a and e_a values. In a recent study, Szilagyi and Schepers [2014] demonstrated the existence of a near-constant wet surface temperature over irrigated crops, supporting the above rationale behind (12). Normally for this small wet patch, the β_{we} is negative when the air is not near saturation, that is, we get the sensible heat flux downward fueling the latent heat flux, thus T_{wes} is typically lower than T_a . Note that when the air is close to saturation, T_{wes} can be larger than T_a ; in such cases T_{wea} should be capped by T_a [Huntington et al., 2011; McMahon et al., 2013; Szilagyi, 2014]. With R_n , G , T_a , and e_a measured by in situ observations,

2006; Ryu et al., 2008]. ψ_v and ψ_m are the stability correction functions for humidity and momentum, respectively. On a daily basis, it is usually assumed that $\psi_v = \psi_m = 0$ due to neutral atmospheric stability [Brutsaert, 2005]. Note that the assumption of $\psi_v = \psi_m = 0$ and $kB^{-1} = 2$ may be invalid in shorter time periods (e.g., $< 1 \text{ h}$) because the effect of atmospheric stability could be important and the roughness lengths would vary markedly with the diurnal variation in land surface temperatures [Brutsaert, 1982; Parlange and Katul, 1992].

As Penman’s Rome wind function (7) was parameterized with wind measurements at a height of 2 m above ground equaling z_2 in (11), a direct comparison between the two wind functions is displayed in Figure 4. The result indicates that (7) tends to overestimate $f(U)$ when the mean daily wind speed is lower than 3.7 m s^{-1} , but it under-

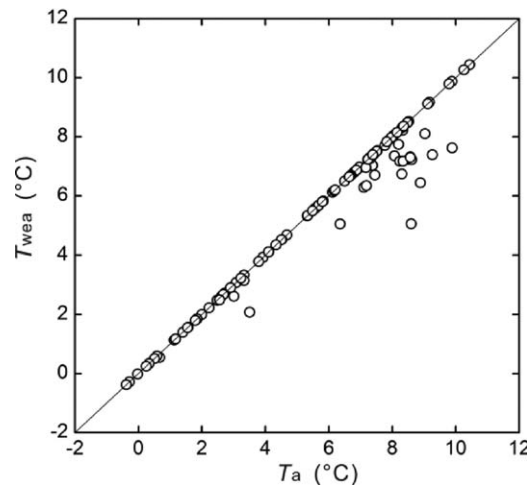


Figure 5. Comparison of daily actual air temperature (T_a) and estimated wet-environment air temperatures (T_{wea}) at SAS. The larger the difference between T_a and T_{wea} , the more arid is the environment.

and ET_{p-c} calculated by (6) and (10), the T_{wes} ($\approx T_{wea}$) could therefore be obtained through an iterative process in (12). Similar to the shrublands of Nevada in the U.S. [Huntington *et al.*, 2011], the difference between T_a and T_{wea} at SAS usually increases with the number of days of elevated T_a (Figure 5).

With T_{wea} estimated, (9) becomes

$$ET_{w-c} = \alpha \frac{\Delta_{wea}(R_n - G)}{\Delta_{wea} + \gamma} \quad (13)$$

where Δ_{wea} ($\text{kPa } ^\circ\text{C}^{-1}$) is the slope of the saturation vapor pressure curve at T_{wea} . ET_{w-c} now is the wet environment evapotranspiration rate calculated with Δ_{wea} in place of Δ .

The most often cited value of 1.26 of the dimensionless Priestley-Taylor coefficient, α , derived by Priestley and Taylor [1972], has no concrete physical significance because it was obtained as an average of a series of field experiments. It may therefore be necessary to specify α for local conditions [Hobbins *et al.*, 2001b; Morton, 1983; Sugita *et al.*, 2001; Xu and Singh, 2005]. Following Kahler and Brutsaert [2006], on wet days when ET_a is close to ET_{p-c} and therefore to ET_{w-c} , α can be estimated from the observed ET_a values. In the present study, it is assumed that whenever ET_a/ET_{p-c} is larger than 0.9, the ET_{w-c} in (13) can be replaced by the observed ET_a , thus α could be recalculated. According to the observed data, there were 8 days in 2013 with ET_a/ET_{p-c} ranging from 0.90 to 1.07, with a mean of 0.95 and a median of 0.92. Hence, an average α value of 1.13 was obtained from these 8 days. This value, smaller than the typically employed 1.26, is close to the fitted results of Szilagyi [2007] and Pettijohn and Salvucci [2006] who used daily flux data from a similar period of the year in the U.S. prairie. Yang *et al.* [2013] found a significant seasonal variation in the value of α , being smaller in summer and larger in winter, mostly due to the impact of the monsoon. The observations in the present study come from June to September when the SAS was influenced by the Southern Asian monsoon, therefore the 1.13 value of α seems realistic.

When ET_{p-c} is calculated by (6), coupled with the wind function of (10), and ET_{w-c} is calculated via Δ_{wea} in (13) with $\alpha = 1.13$, (1) can be rearranged for obtaining an estimate (ET_{a-sim}) of actual evapotranspiration as

$$ET_{a-sim} = (1 + \varepsilon)ET_{w-c}/\varepsilon - ET_{p-c}/\varepsilon \quad (14)$$

6. The Relationship Between Actual and Potential Evapotranspiration

In order to check whether a CR exists at SAS on a daily scale, the relationship between daily ET_a , observed by the in situ ACOS, and the daily ET_p , is discussed below. ET_p is first represented as ET_{p-c} (i.e., calculated by (6) and (10)), then as cE_{pan} , with $c = 1$.

6.1. The Relationship Between Observed ET_a and ET_{p-c}

Daily observed ET_a and estimated ET_{p-c} values are displayed in Figure 6a, against the humidity index, ET_{HI} ($= ET_a/ET_{p-c}$). For a given ET_{HI} , the ET_a and ET_{p-c} values are scattered somewhat randomly due mainly to differences in net radiation. However, with ET_{HI} increasing, ET_a increases as well, while ET_{p-c} does the opposite, indicating an inverse relationship with changes in surface moisture availability. Following Kahler and Brutsaert [2006], we inserted ET_a , ET_{p-c} , ET_{w-c} into (4) and (5), and obtained the dimensionless form of ET_a and ET_{p-c} (Figure 6b). It is clear that the difference between ET_{a+} and ET_{p+} increases with the decrease in ET_{HI} , similar in shape to what Figure 1a depicts.

Since the estimation of ET_{a-sim} using the CR is based on (14), a nested trial-and-error method was employed to optimize the value of ε to reach $\sum \{ET_a - ET_{a-sim}\}^2 = \min$ [Szilagyi, 2007], where ET_a is the observed daily value at SAS. The result, $\varepsilon = 0.995$ (Figure 6b), indicates a symmetric CR in SAS when ET_{p-c} is calculated using

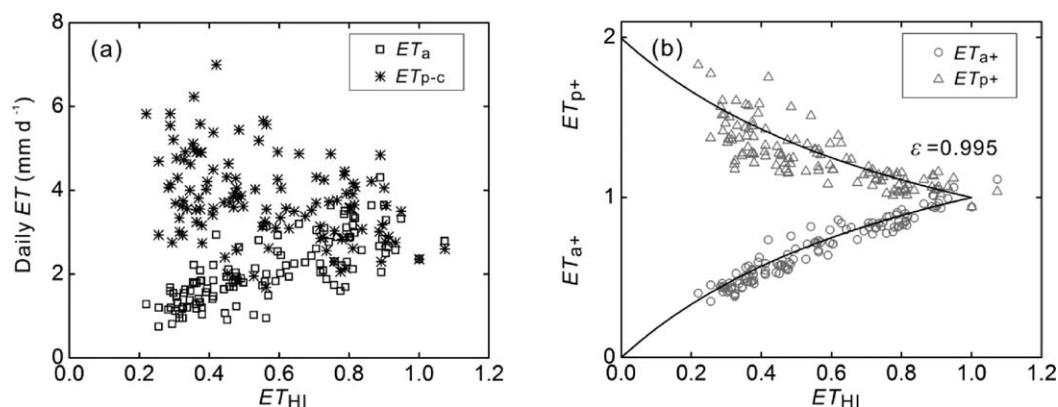


Figure 6. (a) Observed daily actual (ET_a) and estimated daily potential (ET_{p-c}) evapotranspiration rates plotted against the humidity index ($ET_{HI} = ET_a/ET_{p-c}$) at SAS. (b) Normalized daily actual, ET_{a+} ($= ET_a/ET_{w-c}$), and estimated potential, ET_{p+} ($= ET_{p-c}/ET_{w-c}$), evapotranspiration rates plotted against ET_{HI} . The curves represent (4) and (5) with a calibrated value of 0.995 for ϵ .

the Penman method, (6), with the wind function of (10); and ET_{w-c} is calculated using the Priestley-Taylor equation, with $\alpha = 1.13$ and Δ_{wea} evaluated at T_{wea} . Our results contradict previous research which applied the default parameter value of wind function in (7) as well as α and evaluated Δ at T_a in (9), and obtained an asymmetric CR in the semiarid and arid regions of the TP [Wang et al., 2013; Yang et al., 2011; Zhang et al., 2007]. In other words, the local determination of the parameter values within the CR is key to illuminating the true relationship between actual and potential evapotranspiration in the semiarid regions of the TP.

The observation site used for the present study is relatively homogeneous in its fetch in excess of 1 km for the prevailing wind, thus providing almost ideal conditions for the minimal energy advection requirement of the CR. This explains why the calibrated value of ϵ equals 0.995, a value very close to unity. Our symmetric CR in the SAS is also in accordance with the findings of Huntington et al. [2011], who obtained a symmetric CR for Nevada shrublands through a similar calibration of the parameter values.

Since above three calibrations (wind function, T_{wea} , and α) were carried out simultaneously to achieve a symmetric CR in the present study, it may be interesting to distinguish the relative importance of each calibration that when left out, leads to an asymmetric CR. This can be implemented by calibrating only two of three parameter values while keeping the other one unchanged and then searching for the optimized ϵ for each scenario. Figure 7 illustrates that this way the CR becomes asymmetric (explaining why some [Wang et al., 2013; Yang et al., 2011; Zhang et al., 2007], applying no calibration, maintained an asymmetric CR in arid and semiarid region of the TP). Specifically, if the wind function was left uncalibrated, the ϵ became 0.946; when T_{wea} was left uncalibrated, the ϵ became 0.886; and when the $\alpha = 1.26$ was employed, the ϵ became 0.654. This suggests the local calibration of α is most important, followed by the T_{wea} correction, while the wind function may play the smallest role in leading to an asymmetric CR.

6.2. The Relationship Between Observed ET_a and cE_{pan}

With the assumption of $c = 1$ in (8), the daily evaporation rates of the E601B pan at Naqu and the D20 pan at Amdo were used to evaluate the relationship with daily observed ET_a of the SAS (Figure 8). The E_{pan} values in both stations display an inverse relationship with the observed ET_a at SAS when plotted against ET_{HI} (ET_a/cE_{pan}). Moreover, the pan at Amdo (D20 aboveground pan) is more sensitive to changes in ET_a than the one at Naqu (E601B sunken pan) (Figure 8). The reason for this phenomenon will be discussed later.

The CR between observed ET_a and E_{pan} at both Naqu and Amdo becomes more obvious when the dimensionless rates, ET_{a+} ($= ET_a/ET_{w-c}$) and ET_{p+} ($= cE_{pan}/ET_{w-c}$) are plotted against the humidity index, ET_{HI} ($= ET_a/cE_{pan}$), in Figure 9. Employing the E_{pan} data from the two stations and the ET_a values at SAS from 4 June 2013 to 30 September 2013, the nested trial-and-error method was applied again to calibrate ϵ , which became 2.359 for the E601B sunken pan at Naqu, and 3.863 for the D20 aboveground pan at Amdo, both displaying an asymmetric CR when pan evaporation ($c = 1$) rates are used to represent ET_p (Figure 9).

It is not surprising that ϵ is larger than unity for the pans in the present study. This is especially true for the D20 aboveground pan because similar values have already been obtained with class-A aboveground pans,

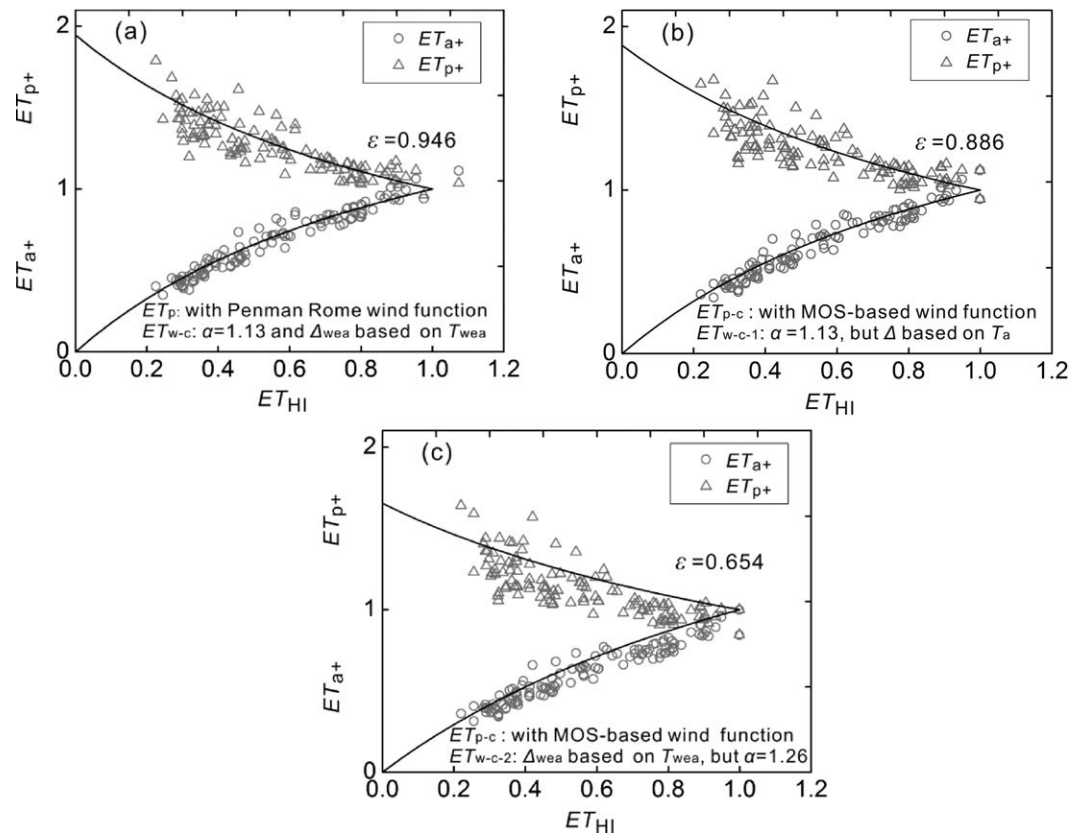


Figure 7. Normalized daily actual and estimated potential evapotranspiration rates plotted against the humidity index, same as in Figure 6b, but only two calibrations were implemented. For (a) without wind function replacement, namely $ET_{a+} (= ET_a/ET_{w-c})$, $ET_{p+} (= ET_p/ET_{w-c})$, $ET_{HI} (= ET_a/ET_p)$; (b) without T_{wea} calibration, namely $ET_{a+} (= ET_a/ET_{w-c-1})$, $ET_{p+} (= ET_p-c/ET_{w-c-1})$, $ET_{HI} (= ET_a/ET_{p-c})$; (c) without α calibration, namely $ET_{a+} (= ET_a/ET_{w-c-2})$, $ET_{p+} (= ET_p-c/ET_{w-c-2})$, $ET_{HI} (= ET_a/ET_{p-c})$. Note that the ET_{w-c} was split to ET_{w-c-1} ($\alpha = 1.13$, but Δ is based on T_a) and ET_{w-c-2} (Δ_{wea} is based on T_{wea} , but $\alpha = 1.26$) to represent only α or T_a as being calibrated, respectively. The black curves represent (4) and (5) with a calibrated value of (a) 0.946, (b) 0.886, (c) 0.654 for ϵ , respectively.

employed as a proxy of ET_p [Kahler and Brutsaert, 2006; Pettijohn and Salvucci, 2009; Szilagyi, 2007; Szilagyi and Jozsa, 2008]. Clearly, the additional solar radiation received by the side of the aboveground pans and the significant heat advection from the surrounding environment due to the pans' small orifice area boost the available energy to the pans. In addition, the dynamics of heat storage of water in the pans may also significantly impact the E_{pan} , especially on a daily scale [Roderick et al., 2009]. However, the value of ϵ for the D20 aboveground pan in the present study is somewhat smaller than the values reported for class-A

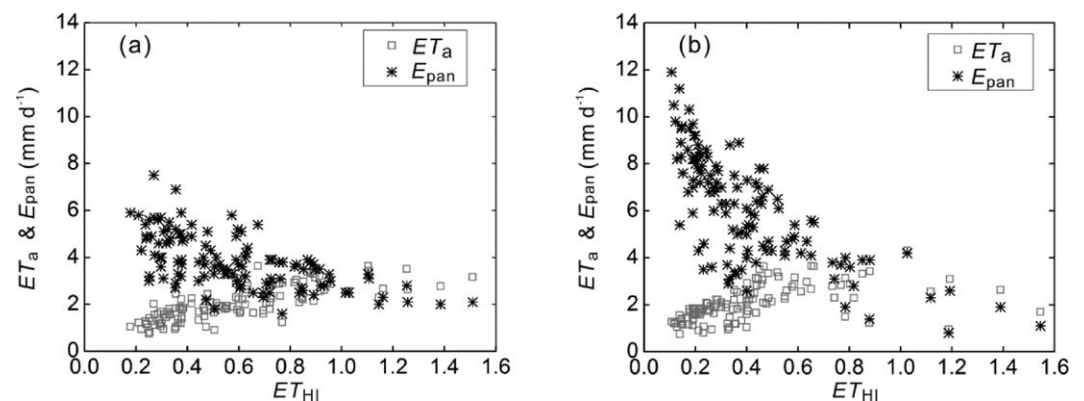


Figure 8. Observed daily actual (ET_a) and estimated daily potential [$ET_p = cE_{pan}$ ($c = 1$)] evapotranspiration rates plotted against the humidity index ($ET_{HI} = ET_a/cE_{pan}$) at SAS. The E_{pan} values are from (a) an E601B sunken pan at Naqu and from (b) a D20 aboveground pan at Amdo.

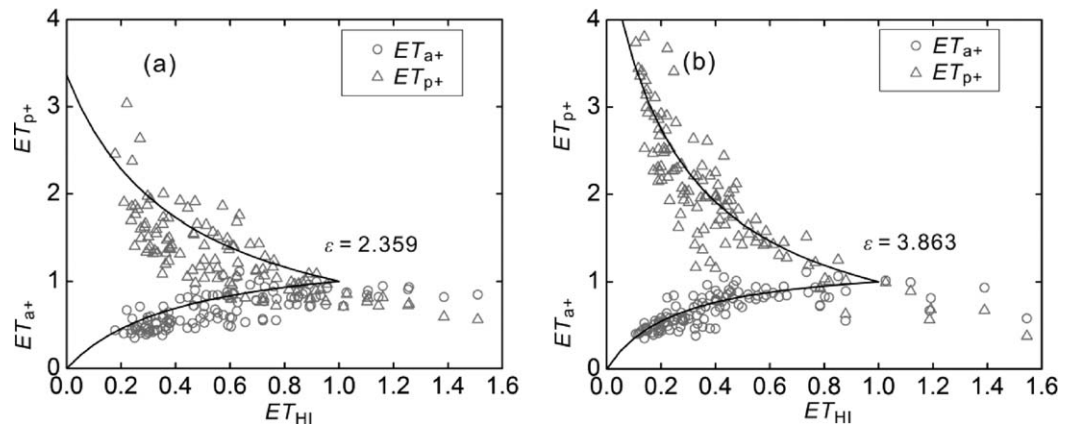


Figure 9. Normalized daily actual, ET_{a+} ($= ET_a/ET_{w-c}$), and estimated potential, ET_{p+} ($= cE_{pan}/ET_{w-c}$, $c = 1$) evapotranspiration rates plotted against ET_{HI} ($= ET_a/cE_{pan}$, $c = 1$). (a) E601B sunken pan at Naqu; (b) D20 aboveground pan at Amdo. The curves represent (4) and (5) with calibrated values of $\epsilon = 2.359$ at Naqu (Figure 9a) and $\epsilon = 3.863$ at Amdo (Figure 9b), respectively.

aboveground pans over the Konza Prairie ($\epsilon = 4.33$) and Little Washita River Basin ($\epsilon = 6.88$) in the U.S. by Kahler and Brutsaert [2006]. This may be caused by differences in the pans' orifice areas and installation.

As the orifice area of the E601B sunken pan is still only 0.3 m^2 , the heat advection cannot be neglected. This leads to its ϵ larger than unity. The reason that the E601B pan is less sensitive than the D20 pan (Figures 8 and 9) is that it is a sunken pan which leads to reduced heat conduction through the side of the pan and therefore decreased diurnal heat storage effect. As shown above, the CR became symmetric when the Penman equation (using MOS for the wind function) was used to estimate ET_{p-c} . It should be noted that Penman [1948] validated his equation using two types of sunken pans: both having a diameter of 0.76 m, but their depths were 0.61 and 1.83 m, respectively. His wind function was later modified (to the so-called Rome wind function of [7]) to give better estimates for plot-sized ponds or wet surfaces, since his original wind function yielded higher ET_p rates due to heat conduction and advection effects, significant for small evaporation pans.

7. Performance of the CR-Based Daily Actual Evapotranspiration Estimates

After deriving the optimized ϵ with observed data from 2013, it is important to test the effectiveness of the CR-based method in a different, verification time period, chosen to be 2012.

7.1. The Penman Method

As discussed in section 6.1, the CR became symmetric ($\epsilon = 0.995$) with the Penman equation using the MOS-derived wind function for the ET_{p-c} estimates and Δ_{wea} evaluated at T_{wea} for the ET_{w-c} estimates. In order to test

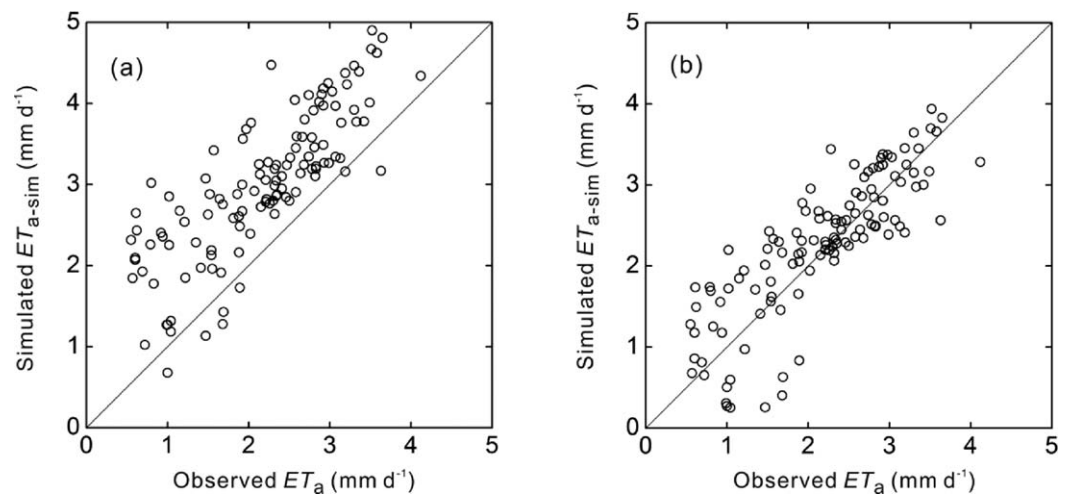


Figure 10. Comparison of daily observed (ET_a) and simulated (ET_{a-sim}) actual evapotranspiration rates from 4 June 2012 to 30 September 2012 at SAS. (a) $ET_{a-sim} = 2ET_w - ET_p$, from (6), (7), and (9) with $\alpha = 1.26$; (b) $ET_{a-sim} = 2ET_{w-c} - ET_{p-c}$, from (6), (10), and (13), with $\alpha = 1.13$.

Table 2. Evaluation of the CR-Based Daily ET_a Estimates in 2012^a

	ETp From Penman, Symmetric CR		ETp From Epan, Asymmetric CR	
	$2ET_w, ET_p$	$2ET_{w-c}, ET_{p-c}$	ET_{w-c}, E_{pan} (E601B)	ET_{w-c}, E_{pan} (D20)
CC	0.804	0.828	0.692	0.742
NSE	-0.352	0.642	-0.450	0.455
MAE	0.86	0.40	0.79	0.48
RMSE	0.994	0.512	1.030	0.631

^aCC, correlation coefficient; NSE, Nash-Sutcliffe efficiency coefficient; MAE, mean absolute error (mm); and RMSE, root-mean-square error (mm).

as 0.86 and 0.994 mm, respectively. The Nash-Sutcliffe efficiency (NSE) coefficient is -0.352 (Table 2), indicating a poor performance of the original AA model. When the wind function in (6) was replaced by the MOS-based approach, (10), and ET_{w-c} was evaluated at T_{wea} using (13) with $\alpha = 1.13$, the MAE and RMSE values decreased to 0.40 and 0.512 mm, respectively (Table 2). The NSE increased to 0.642, indicating a greatly improved agreement with observed daily ET_a in 2012 (Figure 10b).

It is not true only for the SAS that the CR-based estimates can be improved with local calibration of the parameter values. For instance, *Crago et al.* [2010] confirmed that the MOS-based wind function performed better than *Penman's* [1948], in their AA approach over a Kansas grassland [see *Crago et al.*, 2010, Figures 2 and 3]. Besides, *Huntington et al.* [2011] compared the results of their CR-based ET_a estimation method in the shrublands of Nevada, when T_a was replaced by the *Szilagyi and Jozsa* [2008] estimate of T_{wea} to calculate ET_w , and found that the latter improved the ET_a estimates [see *Huntington et al.*, 2011, Figure 9]. Recently, *Szilagyi* [2014] also found the bias of AA model in estimating ET_a in a semiarid savanna in Botswana could be reduced from 53% to 23% when the T_a was replaced with the T_{wea} in calculating the ET_w . In the present study, the employment of an MOS-based wind function, local calibrated α , and T_{wea} together may explain the success of ET_{a-sim} by (14) at SAS (Figure 10b).

7.2. The Pan Evaporation Method

As discussed in section 6.2, the CR is asymmetric with pan evaporation values for ET_p . By insertion of the cE_{pan} ($c = 1$) values into ET_{p-c} of (14), ET_{a-sim} in 2012 was calculated (Figure 11). Note that ϵ is 2.359 for the E601B pan and 3.863 for the D20 pan in (14). The Pearson correlation values between the observed ET_a and ET_{a-sim} are 0.692 and 0.742 when the E601B and D20 pans are used, respectively. The performance of the E601B pan is not as good as that of the D20 pan (Figure 11). The former tends to overestimate ET_a to some extent with MAE and RMSE values of 0.79 and 1.030 mm, respectively, and an NSE of -0.450 (Table 2). This maybe because the local advection influence on the E601B pan at Naqu station in 2012 and 2013 was

the performance of the CR using its original parameter values, called the original AA model, i.e., $ET_{a-sim} = 2ET_w - ET_p$ [*Brutsaert and Stricker*, 1979], (6), (7), and (9) were employed using the data of 2012 (Figure 10a). The daily ET_{a-sim} values are clearly larger than the observed daily ET_a rates, although their correlation is good. The mean-absolute-error (MAE) and root-mean-square-error (RMSE) are as high

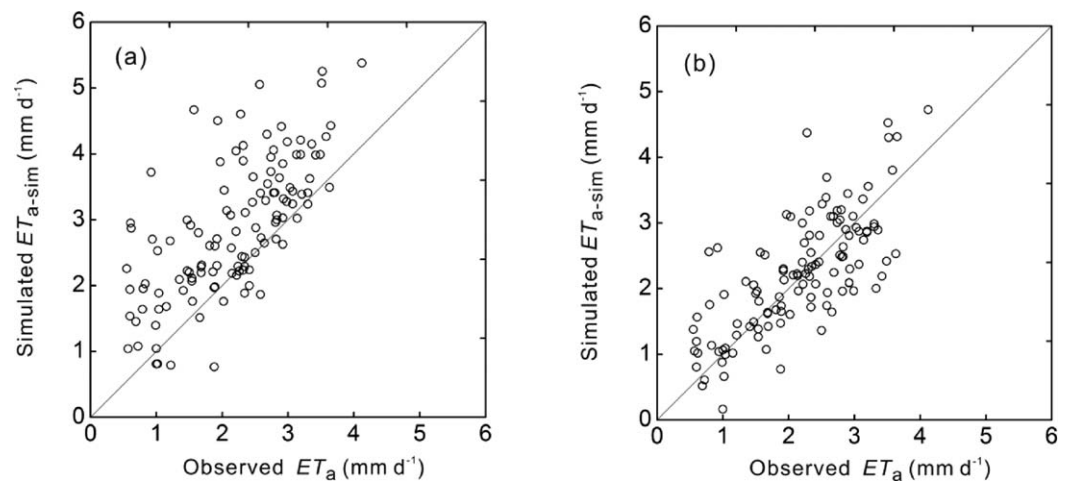


Figure 11. Comparison of daily observed (ET_a) and simulated (ET_{a-sim}) actual evapotranspiration rates from 4 June 2012 to 30 September 2012 at SAS. ET_{a-sim} is from (14) with $ET_{p-c} = cE_{pan}$, $c = 1$, and calibrated values of (a) $\epsilon = 2.359$ for the sunken at Naqu and (b) $\epsilon = 3.863$ for the aboveground at Amdo.

much different, thereby aggravating the variability of the E_{pan} (hence impacting the CR-based method in estimating the $ET_{\text{a-sim}}$) in these 2 years. The D20 pan yielded improved MAE and RMSE values of 0.48 and 0.631 mm, respectively. The NSE is 0.455, indicating a much better performance (Table 2 and Figure 11b).

8. Conclusions

Although *LeDrew* [1979] argued that the CR theory could not be validated for a daily time scale, daily observed actual evapotranspiration and estimated potential evapotranspiration did indeed express complementarity in a semiarid alpine steppe of the TP. This is significant because, with the help of the CR theory, the ET_{a} rates can be estimated from routine meteorological observations, even though TP is known as sparsely observational. Future work should determine the locally calibrated parameter values, similar to the present study, for different vegetation cover types and climatic regions of the TP for ET_{a} estimation methods that employ the CR theory, and thus aiding the work toward a successful estimation of ET_{a} for the entire TP.

With the MOS-based wind function for calculating $ET_{\text{p-cr}}$, a Priestley-Taylor coefficient value of $\alpha = 1.13$, and estimated wet environment air temperature for calculating $ET_{\text{w-cr}}$, the CR became symmetric in a high-altitude semiarid alpine steppe in the TP. Hence, it is believed that previous research [*Wang et al.*, 2013; *Yang et al.*, 2011; *Zhang et al.*, 2007], claiming that the CR is asymmetric in the arid and semiarid regions of the TP, may have resulted simply from employing the original parameter values of the CR-based AA model. The application of the MOS-based wind function as well as an estimate of the wet-environment air temperature together with a local calibration of α , all emphasized by *Brutsaert* [2013], are all recommended as necessary building blocks for the correct evaluation of the CR within the TP. Among them, the local calibration of α is most important, followed by the T_{wea} correction; while the replacement of the classical wind function with an MOS-based one plays the least important role in leading to a symmetric CR. The resulting daily $ET_{\text{a-sim}}$ estimates via the symmetric CR yielded good agreement with the observed daily ET_{a} at the present semiarid alpine steppe.

Daily pan evaporation, E_{pan} , from the two CMA stations employed, displayed a clear inverse trend in comparison with daily observed ET_{a} of the SAS. Radiation received by the side of the pan, nonnegligible heat advection due to the pan's small orifice area [*Szilagyi and Jozsa*, 2008] and the dynamics of heat storage of the pan water [*Roderick et al.*, 2009] led to an asymmetric CR when using E_{pan} for ET_{p} . This is true not only for the D20 aboveground pan but also for the E601B sunken pan, because the effect of heat advection is still present for sunken pans, even if heat conduction is much reduced within the soil. Finally, the D20 aboveground pan performed better than the E601B sunken pan in estimating the actual evapotranspiration rate of a semiarid alpine steppe via the CR theory.

In summary, the benefit of a symmetric CR is that it dispenses with one parameter (ϵ), thus allowing for a simpler calibration and application of the CR in estimating actual evapotranspiration [*Brutsaert*, 2005; *Crago and Qualls*, 2013]. While the current analysis of the CR with E_{pan} does not contribute to the attainment of the symmetry, it provides important clue for historical reasons [*Brutsaert and Parlange*, 1998], since long time series of E_{pan} measurements exist and may be helpful for detecting the trends of terrestrial ET_{a} associated with the long-term climate change.

Acknowledgments

This research was supported by the National Natural Science Foundation of China (41190080), the Strategic Priority Research Program (B) of CAS (XDB03030200), and the Hundred Talents Program of CAS. We are grateful to all members in Zhang's group who had been enrolled in the field work. We thank Tim McVicar for helpful discussions. Special appreciations are given to the Associate Editor and four anonymous reviewers for their valuable comments resulting in an improved manuscript. The pan evaporation data of Naqu station and Amdo station were provided by the China Meteorological Administration. All data for producing the figures can be requested from the corresponding author.

References

- Allen, R. G., L. S. Pereira, T. A. Howell, and M. E. Jensen (2011), Evapotranspiration information reporting: I. Factors governing measurement accuracy, *Agric. Water Manage.*, 98(6), 899–920.
- Biermann, T., W. Babel, W. Ma, X. Chen, E. Thiem, Y. Ma, and T. Foken (2014), Turbulent flux observations and modelling over a shallow lake and a wet grassland in the Nam Co basin, Tibetan Plateau, *Theor. Appl. Climatol.*, 116(1–2), 301–316, doi:10.1007/s00704-013-0953-6.
- Bouchet, R. (1963), Evapotranspiration réelle et potentielle, signification climatique, *Int. Assoc. Sci. Hydrol. Publ.*, 62, 134–142.
- Brutsaert, W. (1982), *Evaporation Into the Atmosphere: Theory, History and Applications*, 299 pp., Springer, N. Y.
- Brutsaert, W. (2005), *Hydrology: An Introduction*, 605 pp., Cambridge Univ. Press, N. Y.
- Brutsaert, W. (2013), Use of pan evaporation to estimate terrestrial evaporation trends: The case of the Tibetan Plateau, *Water Resour. Res.*, 49, 3054–3058, doi:10.1002/wrcr.20247.
- Brutsaert, W., and M. Parlange (1998), Hydrologic cycle explains the evaporation paradox, *Nature*, 396, 30 pp.
- Brutsaert, W., and H. Stricker (1979), An advection-aridity approach to estimate actual regional evapotranspiration, *Water Resour. Res.*, 15(2), 443–450.
- Chen, X., Z. Su, Y. Ma, K. Yang, and B. Wang (2013), Estimation of surface energy fluxes under complex terrain of Mt. Qomolangma over the Tibetan Plateau, *Hydrol. Earth Syst. Sci.*, 17(4), 1607–1618, doi:10.5194/hess-17-1607-2013.
- Crago, R., and R. Crowley (2005), Complementary relationships for near-instantaneous evaporation, *J. Hydrol.*, 300(1–4), 199–211, doi:10.1016/j.jhydrol.2004.06.002.

- Crago, R., and R. Qualls (2013), The value of intuitive concepts in evaporation research, *Water Resour. Res.*, *49*, 6100–6104, doi:10.1002/wrcr.20420.
- Crago, R., R. Qualls, and M. Feller (2010), A calibrated advection-aridity evaporation model requiring no humidity data, *Water Resour. Res.*, *46*, W09519, doi:10.1029/2009WR008497.
- Gao, Q., Y. Wan, H. Xu, Y. Li, W. Jiangcun, and A. Borjigidai (2010), Alpine grassland degradation index and its response to recent climate variability in Northern Tibet, China, *Quat. Int.*, *226*(1–2), 143–150.
- Golubev, V. S., J. H. Lawrimore, P. Y. Groisman, N. A. Speranskaya, S. A. Zhuravin, M. J. Menne, T. C. Peterson, and R. W. Malone (2001), Evaporation changes over the contiguous United States and the former USSR: A reassessment, *Geophys. Res. Lett.*, *28*(13), 2665–2668.
- Gu, S., Y. Tang, X. Cui, M. Du, L. Zhao, Y. Li, S. Xu, H. Zhou, T. Kato, and P. Qi (2008), Characterizing evapotranspiration over a meadow ecosystem on the Qinghai-Tibetan Plateau, *J. Geophys. Res.*, *113*, D08118, doi:10.1029/2007JD009173.
- Han, S., D. Xu, S. Wang, and Z. Yang (2013), Similarities and differences of two evapotranspiration models with routinely measured meteorological variables: Application to a cropland and grassland in northeast China, *Theor. Appl. Climatol.*, *117*(3–4), 501–510.
- Han, S., F. Tian, and H. Hu (2014), Positive or negative correlation between actual and potential evaporation? Evaluating using a nonlinear complementary relationship model, *Water Resour. Res.*, *50*, 1322–1336, doi:10.1002/2013WR014151.
- Hobbins, M. T., J. A. Ramírez, T. C. Brown, and L. H. J. M. Claessens (2001a), The complementary relationship in estimation of regional evapotranspiration: The complementary relationship areal evapotranspiration and advection-aridity models, *Water Resour. Res.*, *37*(5), 1367–1387.
- Hobbins, M. T., J. A. Ramírez, and T. C. Brown (2001b), The complementary relationship in estimation of regional evapotranspiration: An enhanced Advection-Aridity model, *Water Resour. Res.*, *37*(5), 1389–1403.
- Hobbins, M. T., J. A. Ramírez, and T. C. Brown (2004), Trends in pan evaporation and actual evapotranspiration across the conterminous US: Paradoxical or complementary?, *Geophys. Res. Lett.*, *31*, L13503, doi:10.1029/2004GL0198426.
- Huntington, J. L., J. Szilagyi, S. W. Tyler, and G. M. Pohl (2011), Evaluating the complementary relationship for estimating evapotranspiration from arid shrublands, *Water Resour. Res.*, *47*, W05533, doi:10.1029/2010WR009874.
- Jaksa, W. T., V. Sridhar, J. L. Huntington, and M. Khanal (2013), Evaluation of the complementary relationship using Noah Land Surface Model and North American Regional Reanalysis (NARR) data to estimate evapotranspiration in semiarid ecosystems, *J. Hydrometeorol.*, *14*(1), 345–359, doi:10.1175/JHM-D-11-067.1.
- Kahler, D. M., and W. Brutsaert (2006), Complementary relationship between daily evaporation in the environment and pan evaporation, *Water Resour. Res.*, *42*, W05413, doi:10.1029/2005WR004541.
- LeDrew, E. F. (1979), A diagnostic examination of a complementary relationship between actual and potential evapotranspiration, *J. Appl. Meteorol.*, *18*, 495–501.
- Lhomme, J. P., and E. Elguero (1999), Examination of evaporative fraction diurnal behaviour using a soil-vegetation model coupled with a mixed-layer model, *Hydrol. Earth Syst. Sci.*, *3*(2), 259–270.
- Linacre, E. T. (1993), Data-sparse estimation of lake evaporation, using a simplified Penman equation, *Agric. For. Meteorol.*, *64*(3), 237–256.
- Liu, G., Y. Liu, M. Hafeez, D. Xu, and C. Vote (2012), Comparison of two methods to derive time series of actual evapotranspiration using eddy covariance measurements in the southeastern Australia, *J. Hydrol.*, *454*, 1–6.
- Liu, S., R. Sun, Z. Sun, X. Li, and C. Liu (2006), Evaluation of three complementary relationship approaches for evapotranspiration over the Yellow River basin, *Hydrol. Processes*, *20*(11), 2347–2361, doi:10.1002/hyp.6048.
- Ma, Y., S. Kang, L. Zhu, B. Xu, L. Tian, and T. Yao (2008), Roof of the world: Tibetan observation and research platform: Atmosphere-land interaction over a heterogeneous landscape, *Bull. Am. Meteorol. Soc.*, *89*(10), 1487–1492.
- Ma, Y., Z. Zhu, L. Zhong, B. Wang, C. Han, Z. Wang, Y. Wang, L. Lu, P. Amatya, W. Ma, and Z. Hu (2014), Combining MODIS, AVHRR and in situ data for evapotranspiration estimation over heterogeneous landscape of the Tibetan Plateau, *Atmos. Chem. Phys.*, *14*, 1507–1515.
- Mallick, K., A. Jarvis, J. B. Fisher, K. P. Tu, E. Boegh, and D. Niyogi (2013), Latent heat flux and canopy conductance based on Penman-Monteith, Priestley-Taylor Equation, and Bouchet's complementary hypothesis, *J. Hydrometeorol.*, *14*(2), 419–442, doi:10.1175/JHM-D-12-0117.1.
- Mallick, K., et al. (2014), A surface temperature initiated closure (STIC) for surface energy balance fluxes, *Remote Sens. Environ.*, *141*, 243–261.
- Matin, M. A., and C. P. A. Bourque (2013), Assessing spatiotemporal variation in actual evapotranspiration for semi-arid watersheds in northwest China: Evaluation of two complementary-based methods, *J. Hydrol.*, *486*, 455–465.
- McMahon, T. A., M. C. Peel, and J. Szilagyi (2013), Comment on the application of the Szilagyi-Jozsa advection-aridity model for estimating actual terrestrial evapotranspiration in "Estimating actual, potential, reference crop and pan evaporation using standard meteorological data: A pragmatic synthesis" by McMahon et al. (2013), *Hydrol. Earth Syst. Sci.*, *17*, 4865–4867.
- Miehe, G., et al. (2011), Plant communities of central Tibetan pastures in the Alpine Steppe/Kobresia pygmaea ecotone, *J. Arid Environ.*, *75*(8), 711–723, doi:10.1016/j.jaridenv.2011.03.001.
- Monin, A., and A. Obukhov (1954), Basic laws of turbulent mixing in the surface layer of the atmosphere, *Contrib. Geophys. Inst. Acad. Sci. USSR*, *151*, 163–187.
- Morton, F. I. (1983), Operational estimates of areal evapotranspiration and their significance to the science and practice of hydrology, *J. Hydrol.*, *66*(1–4), 1–76.
- Ohmura, A., and M. Wild (2002), Is the hydrological cycle accelerating?, *Science*, *298*, 1345–1346.
- Oliphant, A. J., C. S. B. Grimmond, H. N. Zutter, H. P. Schmid, H. B. Su, S. L. Scott, B. Offerle, J. C. Randolph, and J. Ehman (2004), Heat storage and energy balance fluxes for a temperate deciduous forest, *Agric. For. Meteorol.*, *126*(3–4), 185–201.
- Ozdogan, M., and G. D. Salvucci (2004), Irrigation-induced changes in potential evapotranspiration in southeastern Turkey: Test and application of Bouchet's complementary hypothesis, *Water Resour. Res.*, *40*, W04301, doi:10.1029/2003WR002822.
- Parlange, M. B., and G. G. Katul (1992), An advection-aridity evaporation model, *Water Resour. Res.*, *28*(1), 127–132.
- Penman, H. L. (1948), Natural evaporation from open water, bare soil and grass, *Proc. R. Soc. London, Ser. A*, *193*, 120–145, doi:10.1098/rspa.1948.0037.
- Pettijohn, J. C., and G. D. Salvucci (2006), Impact of an unstressed canopy conductance on the Bouchet-Morton complementary relationship, *Water Resour. Res.*, *42*, W09418, doi:10.1029/2005WR004385.
- Pettijohn, J. C., and G. D. Salvucci (2009), A new two-dimensional physical basis for the complementary relation between terrestrial and pan evaporation, *J. Hydrometeorol.*, *10*(2), 565–574, doi:10.1175/2008JHM1026.1.
- Priestley, C., and R. Taylor (1972), On the assessment of surface heat flux and evaporation using large-scale parameters, *Mon. Weather Rev.*, *100*(2), 81–92.
- Qin, J., K. Yang, S. Liang, and X. Guo (2009), The altitudinal dependence of recent rapid warming over the Tibetan Plateau, *Clim. Change*, *97*, 321–327, doi:10.1007/s10584-009-9733-9.

- Ramírez, J. A., M. T. Hobbins, and T. C. Brown (2005), Observational evidence of the complementary relationship in regional evaporation lends strong support for Bouchet's hypothesis, *Geophys. Res. Lett.*, *32*, L15401, doi:10.1029/2005GL023549.
- Roderick, M. L., M. T. Hobbins, and G. D. Farquhar (2009), Pan evaporation trends and the terrestrial water balance. I. Principles and observations, *Geogr. Compass*, *3*(2), 746–760.
- Ryu, Y., D. D. Baldocchi, S. Ma, and T. Hehn (2008), Interannual variability of evapotranspiration and energy exchange over an annual grassland in California, *J. Geophys. Res.*, *113*, D09104, doi:10.1029/2007JD009263.
- Sugita, M., J. Usui, I. Tamagawa, and I. Kaihotsu (2001), Complementary relationship with a convective boundary layer model to estimate regional evaporation, *Water Resour. Res.*, *37*(2), 353–365, doi:10.1029/2000WR900299.
- Szilagyi, J. (2007), On the inherent asymmetric nature of the complementary relationship of evaporation, *Geophys. Res. Lett.*, *34*, L02405, doi:10.1029/2006GL028708.
- Szilagyi, J. (2014), Temperature corrections in the Priestley-Taylor equation of evaporation, *J. Hydrol.*, *519*, 455–464.
- Szilagyi, J., and J. Jozsa (2008), New findings about the complementary relationship-based evaporation estimation methods, *J. Hydrol.*, *354*(1–4), 171–186, doi:10.1016/j.jhydrol.2008.03.008.
- Szilagyi, J., and J. Jozsa (2009a), Complementary relationship of evaporation and the mean annual water-energy balance, *Water Resour. Res.*, *45*, W09201, doi:10.1029/2009WR008129.
- Szilagyi, J., and J. Jozsa (2009b), Analytical solutions of the coupled 2-D turbulent heat and vapor transport equations and the complementary relationship of evaporation, *J. Hydrol.*, *372*, 61–67.
- Szilagyi, J., and A. Schepers (2014), Coupled heat and vapor transport: The thermostat effect of a freely evaporating land surface, *Geophys. Res. Lett.*, *41*, 435–441, doi:10.1002/2013GL058979.
- Szilagyi, J., M. T. Hobbins, and J. Jozsa (2009), Modified advection-aridity model of evapotranspiration, *J. Hydrol. Eng.*, *14*(6), 569–574.
- van Heerwaarden, C. C., J. V. G. de Arellano, and A. J. Teuling (2010), Land-atmosphere coupling explains the link between pan evaporation and actual evapotranspiration trends in a changing climate, *Geophys. Res. Lett.*, *37*, L21401, doi:10.1029/2010GL045374.
- Wang, H., D. Liu, H. Lin, A. Montenegro, and X. Zhu (2014), NDVI and vegetation phenology dynamics under the influence of sunshine duration on the Tibetan plateau, *Int. J. Climatol.*, *34*, doi:10.1002/joc.4013.
- Wang, K., and R. E. Dickinson (2012), A review of global terrestrial evapotranspiration: Observation, modeling, climatology, and climatic variability, *Rev. Geophys.*, *50*, RG2005, doi:10.1029/2011RG000373.
- Wang, W., W. Xing, Q. Shao, Z. Yu, S. Peng, T. Yang, B. Yong, J. Taylor, and V. P. Singh (2013), Changes in reference evapotranspiration across the Tibetan Plateau: Observations and future projections based on statistical downscaling, *J. Geophys. Res. Atmos.*, *118*, 4049–4068, doi:10.1002/jgrd.50393.
- Wang, Y., B. Liu, B. Su, J. Zhai, and M. Gemmer (2011), Trends of calculated and simulated actual evaporation in the Yangtze River basin, *J. Clim.*, *24*(16), 4494–4507, doi:10.1175/2011JCLI3933.1.
- World Meteorological Organization (WMO) (2008), Measurement of evaporation, in *WMO Guide to Meteorological Instruments and Methods of Observation*, chap. 10, pp. I.10-1–I.10-10., Geneva, Switzerland.
- Wu, G., Y. Liu, B. He, Q. Bao, A. Duan, and F. F. Jin (2012), Thermal controls on the Asian summer monsoon, *Sci. Rep.*, *2*, doi:10.1038/srep00404.
- Xiong, A., J. Liao, and B. Xu (2012), Reconstruction of a daily large-pan evaporation dataset over China, *J. Appl. Meteorol. Climatol.*, *51*(7), 1265–1275, doi:10.1175/JAMC-D-11-0123.1.
- Xu, C., and V. P. Singh (2005), Evaluation of three complementary relationship evapotranspiration models by water balance approach to estimate actual regional evapotranspiration in different climatic regions, *J. Hydrol.*, *308*, 105–121.
- Yang, H., and D. Yang (2012), Climatic factors influencing changing pan evaporation across China from 1961 to 2001, *J. Hydrol.*, *414–415*, 184–193, doi:10.1016/j.jhydrol.2011.10.043.
- Yang, H., D. Yang, and Z. Lei (2013), Seasonal variability of the complementary relationship in the Asian monsoon region, *Hydrol. Processes*, *27*(19), 2736–2741, doi:10.1002/hyp.9400.
- Yang, K., B. Ye, D. Zhou, B. Wu, T. Foken, J. Qin, and Z. Zhou (2011), Response of hydrological cycle to recent climate changes in the Tibetan Plateau, *Clim. Change*, *109*(3–4), 517–534, doi:10.1007/s10584-011-0099-4.
- Yang, Y., J. Fang, Y. Pan, and C. Ji (2009), Aboveground biomass in Tibetan grasslands, *J. Arid Environ.*, *73*(1), 91–95.
- Yao, T., et al. (2012), Different glacier status with atmospheric circulations in Tibetan Plateau and surroundings, *Nat. Clim. Change*, *2*, 663–667, doi:10.1038/nclimate1580.
- Ye, D., and G. Wu (1998), The role of the heat source of the Tibetan Plateau in the general circulation, *Meteorol. Atmos. Phys.*, *67*(1–4), 181–198.
- Yin, Y., S. Wu, and D. Zhao (2013), Past and future spatiotemporal changes in evapotranspiration and effective moisture on the Tibetan Plateau, *J. Geophys. Res. Atmos.*, *118*, 10,850–10,860, doi:10.1002/jgrd.50858.
- Yu, J., Y. Zhang, and C. Liu (2009), Validity of the Bouchet's complementary relationship at 102 observatories across China, *Sci. China Ser. D*, *52*(5), 708–713, doi:10.1007/s11430-009-0066-3.
- Zhang, Y., C. Liu, Y. Tang, and Y. Yang (2007), Trends in pan evaporation and reference and actual evapotranspiration across the Tibetan Plateau, *J. Geophys. Res.*, *112*, D12110, doi:10.1029/2006JD008161.
- Zheng, J., J. Bian, Q. Ge, Z. Hao, Y. Yin, and Y. Liao (2013), The climate regionalization in China for 1981–2010, *Chin. Sci. Bull.*, *58*, 3088–3099, doi:10.1360/972012-1491.
- Zou, X., S. Li, C. Zhang, G. Dong, and Y. Dong (2002), Desertification and control plan in the Tibet Autonomous Region of China, *J. Arid Environ.*, *51*(2), 183–198, doi:10.1006/jare.2001.0943.